Sādhanā (2022)47:125
https://doi.org/10.1007/s12046-022-01885-4

Transient analysis and parameter estimation with optimizations in a plate heat exchanger

PRAGYA TIWARY, PRABHA NISHA TOPPO and ARNAB KARMAKAR*

Department of Chemical Engineering, Birla Institute of Technology, Mesra, Jharkhand 835215, India
e-mail: arnabkarmakar@bitmesra.ac.in

MS received 26 July 2021; revised 23 March 2022; accepted 8 April 2022

Abstract. Transient analysis in a plate heat exchanger is an effective method to study its dynamic behavior. It can extract various performance parameters of a heat exchanger, such as heat transfer coefficient, individual channel flow rate, and time constant. The present work studied the transient response of cold-side water temperature in a U-type, chevron-corrugated countercurrent plate heat exchanger with the step changes of the inlet flow rate of hot-side water. During the experimental temperature transients, the time constants varied from 69.70 to 95.72 s. The calculated overall heat transfer coefficients from the transient experiment were in the range from 1387.99 to 1925.51 W m^{-2} $°C^{-1}$. The transient responses of outlet temperatures were optimized through a time-domain model formulation with parameter estimation techniques. The overall heat transfer coefficients were estimated from the optimized simulations based on a simplex optimization and a nonlinear programming solver. The simplex optimization method underpredicted the experimental transient response with lower values of the predicted heat transfer coefficient. The nonlinear programming solver predicted the transient response precisely with lower values of square sum error.

Keywords. Plate heat exchanger; transient analysis; heat transfer coefficient; parameter estimation; simplex optimization.

1. Introduction

Nowadays, a plate heat exchanger (PHE) is a choice for the chemical, petrochemical, food, and power industries due to its compactness and efficient heat transport capabilities. The compact devices are employed for various purposes, like, pasteurization, sterilization, cooling and boiling in food and beverage industries, cooling and boiling in energy and power plants, waste heat recovery in petrochemicals and refinery, etc. [1]. The PHE typically replaces its counterpart shell and tube type heat exchanger in those industries for its compactness, higher surface volume ratio, a higher percentage of heat recovery, lower requirement of floor space, and ease of maintenance [1, 2].

In recent years, innovations have been made in the plate surface by corrugation technology of various kinds—printed circuit compact heat exchanger and corrugated plate compact heat exchangers of constant amplitude and roughness [1, 3, 4]. It enhances turbulence and heat transfer rate in a plate heat exchanger. A compact heat exchanger with chevron-angled plates produces a higher degree of turbulence with mixing that enhances the heat transfer coefficient. It is more effective than fin-tube and spiral tube compact heat exchangers. With the development of brazed plate technology instead of gasket type plate, the compact heat exchangers are employed in two-phase applications such as refrigeration, vapor generation, heating with boiling, and cooling with condensation [1].

Study and analysis of transient behavior in a heat exchanger are essential to provide safe operations during transients like the changes of set-points, loads, and start-up or shut down of a plant integrated with the heat exchanger. The overall dynamics of a process plant are dependent on the heat exchanger dynamics. The transient response of a counterflow heat exchanger was studied for a gas turbine regenerator [5]. The temperature transient was analyzed with four independent variables including the number of transfer units, wall capacitance ratio, and dimensionless time scales. The transient temperature responses in a heat exchanger with change in temperature and flow rate of other side fluid (shell or tube side) were studied elaborately [6–9].

The temperature responses during transients were experimented with and predicted by an axial dispersion model for a PHE with extensive analysis [10, 11]. The deviation from an ideal plug flow was taken into consideration. The flow maldistributions in plate heat exchangers with U and Z type flow configurations were studied [12]. The study was for the thermal performance of the plate heat exchanger. It was concluded that the flow maldistribution

*For correspondence
Published online: 28 June 2022

and phase lag had significant roles in the transients. The transient responses in one-two and two-two pass plate heat exchangers were predicted [13]. The model considered the ideal plug flow and axial heat dispersion. For the prediction of the dynamic behavior of multi-pass shell and tube heat exchangers, an effective model was presented [14]. The analysis was developed for the parallel and counter flow heat exchangers when these were exposed to the disturbances in step flow and temperature variations. It also included the effect of flow maldistribution on the transients and the influence of heat capacity for nonzero initial conditions. A transient study was carried out in a PHE considering the maldistribution of flow and axial dispersion with a step increase in inlet temperature [15].

The transient analysis and the optimizations are the effective means of parameter estimations that are not frequently available in a field of study. The kinetic parameters were estimated with the help of optimizations of the experimental transients of different chemically reacting systems [16, 17]. The heat transfer coefficients were estimated from the temperature transients during quenching experiments using water and ethylene glycol [18]. The heat transfer coefficients were predicted using the sequential function specification method based on an inverse heat transfer coefficient problem, and the least square function was minimized during each iteration [18]. The reservoir parameters were estimated from the reservoir temperature transients and an optimal regression model [19]. The local heat transfer coefficient and local temperature were estimated in a steam header using the experimental temperature transients and a Bayesian inference-based inverse technique [20].

The present work aims to analyze the experimental transient response of fluid temperature in a U-type, chevron-corrugated countercurrent plate heat exchanger with the step changes of inlet flow rate. A model in the domains of time and space was developed to simulate the transient response of the plate heat exchanger. The outlet water temperature responses in the plate heat exchanger with step changes of opposite side water flow rate were experimented and optimized through parameter estimation techniques. Experimental overall heat transfer coefficients were calculated from the transient experiment, and these have been compared with estimated counterparts obtained by the optimizations.

2. Experimental set-up and procedures

A countercurrent plate heat exchanger with U-flow configuration and chevron type corrugation (Make: Alfa Laval) was used for transient analysis in figure 1. The heated water was circulated in the vertically up-flow channels and cold water was circulated at room temperature in the vertically down-flow channels of the PHE by two centrifugal pumps. The water on both sides of the PHE was taken from a tap. A thermostatic bath was used to heat water to the desired temperature with a maximum temperature of 60°C. The specifications of the plate heat exchanger are given in table 1. For the measurement of water temperature, two thermocouples were placed at the hot side inlet and outlet, whereas the other two thermocouples were at the cold side inlet and outlet. The two rotameters were used to measure the flow rates of cold and hot side fluids. For the experimental study of the transients, two gate valves were used upstreams of the hot side and cold side to regulate the hot and cold flow rates, respectively. The regulated flow rates for both sides were from 0.10 to 0.30 $m^3\ h^{-1}$. The experimental transient analysis was performed with step change of flow rate of one side (hot or cold side) by sudden closing

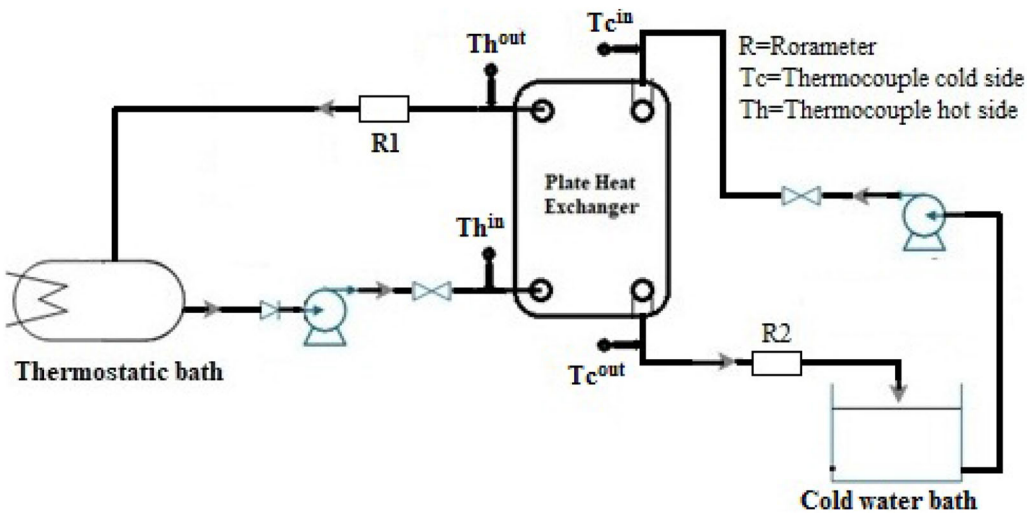

Figure 1. The experimental facility for transient analysis in a plate heat exchanger.

Table 1. Specifications of the plate heat exchanger.

Component	Specification
Rubber gasket material	Nitrile
Plate width inside gasket, L_{wd} (mm)	100
Vertical distance between centers of ports, L_{ver} (mm)	355
Horizontal distance between centers of ports, L_{hor} (mm)	60
Port diameter, D_p (mm)	30
Number of plates N_P	10
Heat exchanger area, A (m^2)	0.3
Mean channel spacing, b (mm)	2.8
Gap between two consecutive plates, (mm)	2.4
Corrugation pitch, P_c (mm)	14.2
Plate thickness, z (mm)	0.5
Plate pitch, p (mm)	2.8
Gasket width, (mm)	7.4
Gasket thickness, (mm)	0.37
Chevron angle, $\beta(^\circ)$	30

Table 2. Operating conditions of the experimental transient analysis.

Sl. no	$\dot{m}_c^{in}(\times 10^2)$ (kg s^{-1})	$\dot{m}_h^{in}(\times 10^2)$ (kg s^{-1})	T_c^{in} (^oC)	T_c^{out} (^oC)	T_h^{in} (^oC)	T_h^{out} (^oC)
1.	6.94	6.88	18	20	60	58
2.	6.94	6.88	15	17	55	53.1
3.	4.16	5.51	15	16	55	53.5
4.	4.15	2.74	30	33.1	55	53.3
5.	6.91	6.55	27.3	29	58	56
6.	6.92	5.45	24	26.1	60	58

(step reduction) and sudden opening (step increase) of the gate valves at the respective side.

The thermostatic bath was filled with tap water and heated at the desired temperature for the hot water circulation at the PHE. The cold water was directly taken from the tap and filled in a tank. The temperature of the tap water in the tank was noted initially. The apparatus was turned on. The pumps were started to circulate hot water and cold water inside the PHE. The two temperature sensors were attached at the outlets to measure the outlet temperatures of the cold and hot sides. The two temperature sensors were placed at the inlets to measure the inlet temperatures of the hot water and cold water. After the attainment of steady state temperatures in the PHE, a step-change in the flow rate was given in the hot side of the PHE by a sudden change of position of the gate valve at the inlet. The cold side outlet temperature of the PHE was noted down with a regular time interval until the steady state was attained. The operating conditions of the PHE are given in table 2. The cold-water inlet temperature was in the range of 15–30°C, whereas the hot-water inlet temperature was in the range of 55–60°C. In the steady states, the temperature and flow rate were maintained at constant levels. The inlet mass flow rates of cold water were in the range from 4.15×10^{-2} to 6.94×10^{-2} kg s^{-1}, whereas the inlet mass flow rates of hot water were in the range from 2.74×10^{-2} to 6.88×10^{-2} kg s^{-1}. It is mentioned that the inlet mass flow rates of hot water and cold water are distributed among hot channels (4 nos.) and cold channels (5 nos.), respectively. The channel mass flow rates of cold water were in the range from 4.93×10^{-4} to 8.25×10^{-4} kg s^{-1}, whereas the channel mass flow rates of hot water were in the range from 3.25×10^{-4} to 8.18×10^{-4} kg s^{-1}.

Table 3. Constants for the correlation for single-phase heat transfer coefficient [2, 21].

β (°)	$Re = \frac{D_h G}{\mu}$	C_h	n
≤30	≤10	0.718	0.349
	> 10	0.348	0.663

3. Experimental determination of heat transfer coefficient

In this section, the calculated film heat transfer coefficients of the hot and cold sides are demonstrated using a developed correlation [21]. The overall heat transfer coefficients of the PHE were calculated using the film heat transfer coefficients. The correlation for single-phase heat transfer coefficient in a gasket-type PHE is given by the following correlation [2, 21]:

$$\frac{hD_h}{k} = C_h \left(\frac{D_h G}{\mu}\right)^n \left(\frac{c_p \mu}{k}\right)^{0.33} \left(\frac{\mu}{\mu_w}\right)^{0.17} \quad (1)$$

where D_h is the hydraulic diameter of the channels, G is the fluid mass velocity, and h is the film heat transfer coefficient. The specific heat capacity, thermal conductivity, and viscosity of the fluid are given by c_p, k, and μ, respectively. The correlation constants C_h and n are presented in table 3.

The single-phase heat transfer area A_1 in a PHE is given by,

$$A_1 = \frac{A_e}{N_e} \quad (2)$$

A_e is the effective area and N_e is the effective number of plates ($N_e = N_P - 2$). The projected plate area A_p is given by,

$$A_p = (L_{ver} - D_p)(L_{hor} + D_p) \quad (3)$$

An enlargement factor ϕ is defined by,

$$\phi = \frac{A_1}{A_p} \tag{4}$$

The hydraulic diameter of each plate channel is given by,

$$D_h = \frac{2b}{\phi} \tag{5}$$

where b is the mean channel spacing. The mass velocity of each channel in the PHE is given by,

$$G = \frac{\dot{m}}{N_{cp} b L_w} \tag{6}$$

where $\dot{m}$ is the mass flow rate of fluid and N_{CP} is the number of channels per pass $= (N_P - 1)/2$.

The overall heat transfer coefficient U is expressed by,

$$\frac{1}{U} = \frac{1}{h_h} + \frac{1}{h_c} + \frac{t}{k_w} \tag{7}$$

where t is the thickness and k_w is the thermal conductivity of the metal wall. The experimental heat transfer coefficients are demonstrated in the result and discussion section.

It is mentioned that the film heat transfer coefficients were calculated using a conventional method based on the steady state temperatures and flow rates of both side fluids. Here, the two steady state temperatures were considered before and after the transients. The two temperatures were averaged to consider for the calculations of the fluid properties and the dimensionless numbers in the correlation.

4. Dynamic modeling of plate heat exchanger

The plate heat exchanger in our study is a vertical countercurrent with a U-flow configuration and chevron-corrugated. There are five channels for the cold fluid passes and four channels for the hot fluid passes with ten plates presented in figure 2. The simplified energy balance equations for the cold side and hot side of the countercurrent plate heat exchanger can be developed based on the following assumptions: (1) the fluid flow is one dimensional and steady, (2) the thermo-physical properties of the hot and cold fluids along the channels are constant, (3) the flow is steady, i.e., velocities of the hot and cold fluids in the channels are constant, (4) because of the very narrow channel, the temperature distributions in the fluid normal to the plate surface are neglected, (5) the conductive heat transfer parallel to the flow direction is neglected which is very lower compared to the convective heat transfer in the same direction, (6) the viscous heat dissipation is neglected and (7) the flow maldistribution and heat transfer due to axial dispersion are neglected.

In the channel nos. i = 1, 3, 5, 7, and 9, the cold water is flowing vertically downward, whereas in the channel nos. i = 2, 4, 6, and 8, the hot water is flowing vertically upward. The energy balance equations in space and time domains can be written for the nine channels in the following:

Channel no. 1

$$\frac{\partial T_i}{\partial t} = -v_c \frac{\partial T_i}{\partial x} + \left(\frac{UA}{mc_p}\right)_c (T_{i+1} - T_i) \tag{8}$$

Channel nos. 3, 5 and 7

$$\frac{\partial T_i}{\partial t} = -v_c \frac{\partial T_i}{\partial x} + \left(\frac{UA}{mc_p}\right)_c (T_{i+1} - 2T_i + T_{i-1}) \tag{9}$$

Channel no. 9

$$\frac{\partial T_i}{\partial t} = -v_c \frac{\partial T_i}{\partial x} + \left(\frac{UA}{mc_p}\right)_c (T_{i-1} - T_i) \tag{10}$$

Channel nos. 2, 4, 6 and 8

$$\frac{\partial T_i}{\partial t} = v_h \frac{\partial T_i}{\partial x} - \left(\frac{UA}{mc_p}\right)_h (2T_i - T_{i-1} - T_{i+1}) \tag{11}$$

$$v_c = p_1; \left(\frac{UA}{mc_p}\right)_c = p_2; v_h = p_3; \left(\frac{UA}{mc_p}\right)_h = p_4 \tag{12}$$

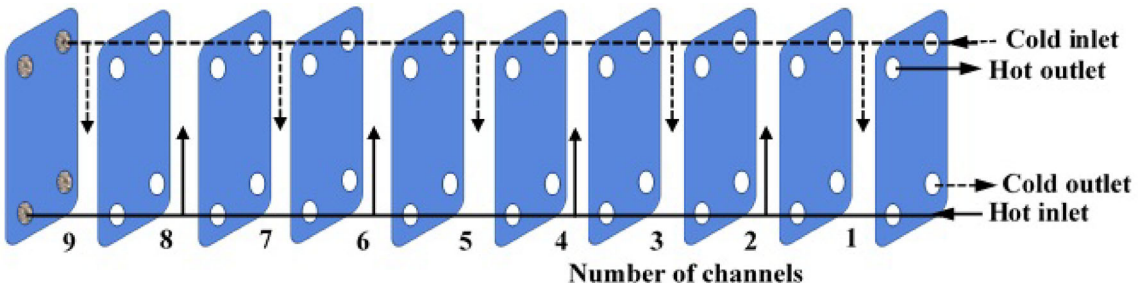

Figure 2. Schematic diagram of flow pattern in the countercurrent plate heat exchanger with U-flow configuration.

p_1, p_2, p_3, and p_4 are parameters for the plate heat exchanger system. The set of partial differential equations of nine equations (for channel nos. i = 1, 2, 3, …, and 9) was discretized using a finite difference scheme to form a set of nine linear equations of the following form:

$$CT = D \tag{13}$$

where C is a tridiagonal coefficient matrix of order nine, D is a column vector of the same order and T is the solution vector of the nine-channel temperatures.

4.1 *Simplex method for optimization*

The parameters were estimated using the simplex method of optimization implemented by Nelder and Mead [22]. At first, five vertices (= $q + 1$) were formed of a pentagon. Here, q is the number of parameters. The one vertex is assumed to be X_0. The other vertices were initialized by the following expressions [23]:

$$\begin{aligned} X_i &= X_0 + \frac{a}{q\sqrt{2}}\left(\sqrt{q+1} + q - 1\right)u_i \\ &\quad + \sum_{j=1, j\neq i}^{n} \frac{a}{q\sqrt{2}}\left(\sqrt{q+1} - 1\right)u_j \\ i &= 1, 2, \ldots, 4 \end{aligned} \tag{14}$$

Here, u_i and u_j are the unit vectors along the ith and jth coordinates, respectively, and a is the size of a polygon in q dimensional space. It computed the objective functions at the vertices, and the polygon moved toward the optimum point through an iterative process. The movement of the simplex is governed by three operations, such as reflection, contraction, and expansion. In each iteration, the computation estimated the maximum point X_{max} and centroid of all points X_c except the maximum one. It replaced the maximum point with three points called, reflection X_r, contraction X_s, and expansion X_e which are given by the following expressions:

$$X_r = (1 + \alpha)X_c - \alpha X_{max} \tag{15}$$

$$X_s = X_c + \beta(X_r - X_c) \tag{16}$$

$$X_e = X_c + \gamma(X_r - X_c) \tag{17}$$

where α, β, and γ are the coefficients of reflection, contraction, and expansion, respectively. Initial values of three coefficients were assumed at the start of the iteration, later these were to be evaluated in each iteration by the followings:

$$\alpha = \frac{[X_r X_c]}{[X_{max} X_c]};\ \alpha > 0 \tag{18}$$

$$\beta = \frac{[X_e X_c]}{[X_{max} X_c]};\ 1 \geq \beta \geq 0 \tag{19}$$

$$\gamma = \frac{[X_e X_c]}{[X_r X_c]};\ \gamma > 1 \tag{20}$$

The objective function in the PHE system is square sum error SSE of all state variables, i.e., nine temperatures of fluid in each channel.

$$SSE = \sum_{i=1}^{i=9} w_i \left(T_i^{sim} - T_i^{exp}\right)^2 \tag{21}$$

The temperature of each channel, T_i^{sim} was evaluated using the simulation of nine partial differential equations (Eqs. 8–11), and T_i^{exp} is the temperature obtained during experimental transient analysis. Here, w_i is the weightage factor for each channel.

$$w_i = \frac{\dot{m}_i}{\sum_{i=1}^{i=9} \dot{m}_i} \tag{22}$$

where $\dot{m}_i$ is the mass flow rate of each channel. It is mentioned that the calculated values of objective functions determine the maximum point where the value of the function was determined to be the highest. The calculation of the points is sensitive to the initial points of the vertices and X_0. A significant deviation in the values of the objective function was observed with a small change of the initial points. The initial value for each run was adjusted in such a way that resulted in a minimum value of the objective function. The transient simulation with the simplex optimization scheme was carried out using a developed code of Matlab® (R2020b) compiler.

4.2 *Optimization based on time-domain model and nonlinear programming solver*

The time-domain model of the PHE has been developed by transforming the set of energy balance equations (Eqs. 8–11) into ordinary differential equations with finite difference discretization. The assumptions of the lumped system are following: (1) the fluid in the channel is well mixed, (2) the temperature of the fluid in a specific channel T_i is uniform along the channel length, (3) the thermophysical properties of the fluid along the flow path of the PHE remain constant. The energy balance equations of the fluid in the nine channels can be represented by the following equations:

Channel no. 1

$$\frac{dT_i}{dt} = -v_c \frac{T_i - T_c^{in}}{\Delta x} + \left(\frac{UA}{mc_p}\right)_c (T_{i+1} - T_i) \tag{23}$$

Channel nos. 3, 5 and 7

$$\frac{dT_i}{dt} = -v_c \frac{T_i - T_c^{in}}{\Delta x} + \left(\frac{UA}{mc_p}\right)_c (T_{i+1} - 2T_i + T_{i-1}) \quad (24)$$

Channel no. 9

$$\frac{dT_i}{dt} = -v_c \frac{T_i - T_c^{in}}{\Delta x} + \left(\frac{UA}{mc_p}\right)_c (T_{i-1} - T_i) \quad (25)$$

Channel nos. 2, 4, 6 and 8

$$\frac{dT_i}{dt} = v_h \frac{T_i - T_h^{in}}{\Delta x} - \left(\frac{UA}{mc_p}\right)_h (2T_i - T_{i-1} - T_{i+1}) \quad (26)$$

$$\frac{v_c}{\Delta x} = p_1; \left(\frac{UA}{mc_p}\right)_c = p_2; \frac{v_h}{\Delta x} = p_3; \left(\frac{UA}{mc_p}\right)_h = p_4 \quad (27)$$

In the set of equations (Eqs. 23–26), parameters p_1, p_2, p_3, and p_4 are optimized using a nonlinear programming solver (NPS) with Matlab® (R2020b) function *fminsearch*, where the objective function is square sum error SSE of all state variables, i.e., 9 temperatures of fluid in each channel depicted in Eq. (21). The nonlinear programming solver was constructed based on Matlab® (R2020b) function *fminsearch* that utilizes the Nelder-Mead [22] simplex algorithm with a pentagon of five vertices (= $q + 1$). The vector X_0 was initialized as one of the vertices of the pentagon and iterated based on the movements of the pentagon with the three consecutive steps of reflection, contraction, and expansion**.** In each iteration, the fluid temperature of each channel T_i was computed based on time-domain ordinary differential equations (Eqs. 23–26), and the objective function (Eq. 21) was calculated. The objective function is minimized based on Matlab® (R2020b) function *fminsearch* that gives the optimized values of parameters p_1, p_2, p_3, and p_4. On the other hand, the simplex method of optimization in section 4.1 was based on time-domain partial differential equations (Eqs. 8–11) and user-defined routines of simplex optimization. The simplex method of optimization based on time-domain partial differential equations is more realistic as it can compute the time delay of the fluid temperature due to its temperature distribution terms. It is more acceptable and accurate for distributed-parameter systems. On the other hand, the NPS can handle the lumped system where temperature distributions in the channels were neglected and outlet fluid temperate of the channel was assumed to be the same as the fluid temperature inside the channel.

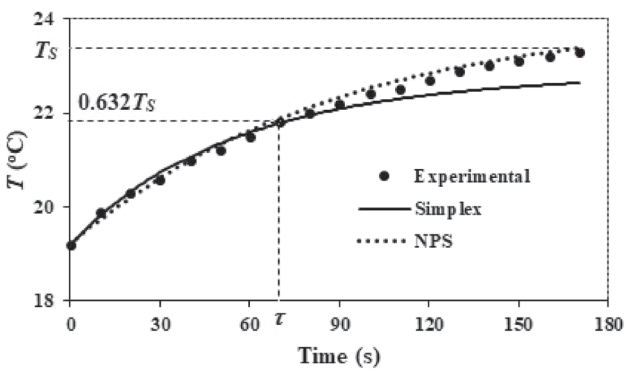

Figure 3. Transient response of cold side outlet temperature of water in the PHE for a positive step change of hot side water flow rate (6.56 + 0.27) × 10^{-2} kg s^{-1} with $\dot{m}_c^{in}$= 6.93 × 10^{-2} kg s^{-1}; T_c^{in}= 18°C; T_h^{in} = 60°C.

5. Results and discussion

In this section, the experimental transient responses of cold side water temperatures in the PHE for the step changes of the hot side water flow rate are discussed with two optimization methods. The experimental transients were simulated with the help of the developed time-domain models and the optimization techniques depicted in the previous section. The first model (Eqs. 8–11) was based on the distributed-system model, whereas the second model was based on the lumped-system assumption with ordinary differential equations (Eqs. 23–26). The transient simulation based on the simplex method was carried out for different values of optimization parameters given by, a= 0.0001; q= 4; X_0= 0.001; α = 1.0; β = 0.5; γ = 2.0. Figure 3 shows the transient response of cold side outlet temperature of water for a positive step change of hot side water flow rate (6.56 + 0.27) × 10^{-2} kg s^{-1}, while cold water flow rate was 6.93 × 10^{-2} kg s^{-1}. The outlet temperature of the cold side water reached close to a steady state at 170 s. Considering the system behaves like a first-order system, the time constant $\tau\left(=\frac{mc_p}{UA}\right)$ of the response corresponds to the time scale at which the temperature response reaches 63.2% of the ultimate steady state T_s. It was estimated as 69.70 s with the help of the graphical technique. The time constant of a heat exchanger quantifies how fast the transient response moves from the initial steady-state to the final steady-state with the step changes in the temperature and flow rate. It is the important parameter for the transient operations during the step change of the operating variables and is frequently encountered in the process industry. The heat transfer coefficient increases with the increase in flow rate. It increases the temperature of the cold side fluid. The simulated transients have been demonstrated for both the simplex and NPS methods in the figure. The NPS method matches the transient response closely with the lower value of SSE while the simplex method of optimization deviates much away compared to the former one with a higher value of SSE. The estimated heat transfer coefficients are represented in table 4 and are discussed at the end of this section. Figure 4 shows the transient response of cold side outlet temperature of water for a positive step change of hot side water flow rate (5.48 + 1.37) × 10^{-2} kg s^{-1}, while

Table 4. Comparisons of the overall heat transfer coefficient by the experimental technique and the optimization methods.

T_h^{in} (°C)	T_c^{in} (°C)	$\dot{m}_h^{in}$ ($\times 10^2$) (kg s^{-1})	$\dot{m}_c^{in}$ ($\times 10^2$) (kg s^{-1})	U_{exp} (W m^{-2} °C^{-1})	$U_{simplex}$ (W m^{-2} °C^{-1})	SSE	U_{NPS} (W m^{-2} °C^{-1})	SSE
60	18	6.56 + 0.27	6.93	1768.47	1057.86	2.35	1548.45	0.08
55	15	5.48 + 1.37	6.93	1775.74	1895.03	90.95	6407.38	7.73
55	15	2.74 + 2.74	4.16	1387.99	1019.37	20.52	2136.86	0.50
58	20	6.84 − 0.27	6.92	1925.51	559.83	5.11	1833.82	0.63
60	15	6.83 − 1.37	6.94	1806.07	438.80	56.81	2759.55	3.30

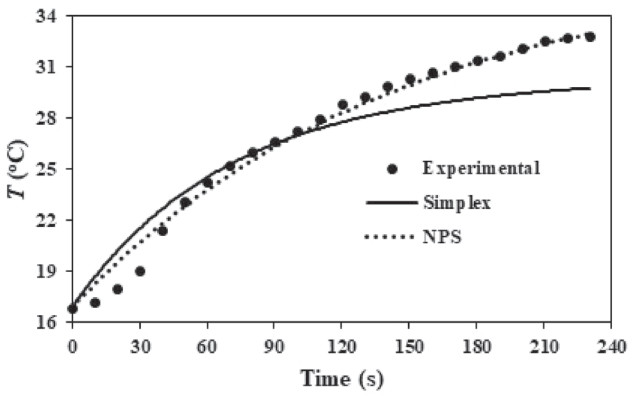

Figure 4. Transient response of cold side outlet temperature of water in the PHE for a positive step change of hot side water flow rate (5.48 + 1.37) × 10^{-2} kg s^{-1} with $\dot{m}_c^{in}$ = 6.93 × 10^{-2} kg s^{-1}; T_c^{in} = 15°C; T_h^{in} = 55°C.

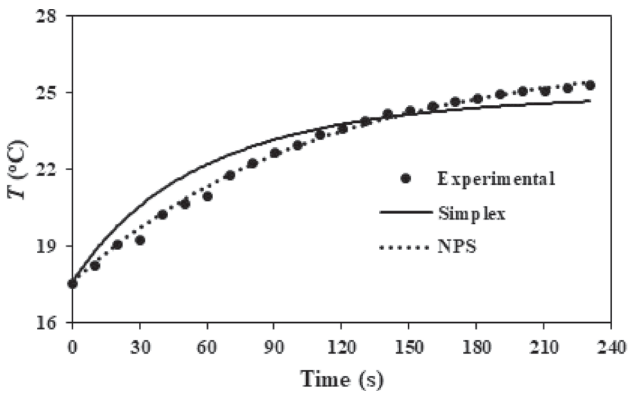

Figure 5. Transient response of cold side outlet temperature of water in the PHE for a positive step change of hot side water flow rate (2.74 + 2.74) × 10^{-2} kg s^{-1} with $\dot{m}_c^{in}$ = 4.16 × 10^{-2} kg s^{-1}; T_c^{in} = 15 °C; T_h^{in} 55°C.

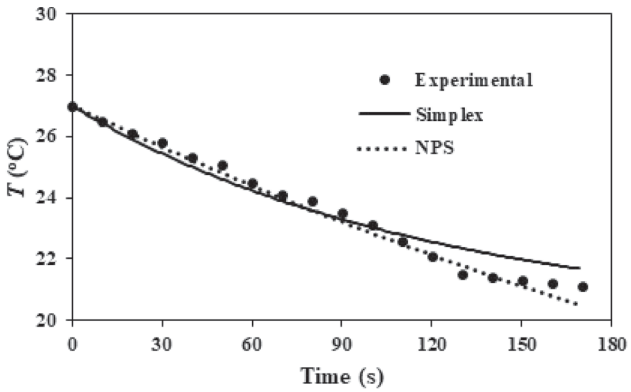

Figure 6. Transient response of cold side outlet temperature of water in the PHE for a negative step change of hot side water flow rate (6.84 − 0.27) × 10^{-2} kg s^{-1} with $\dot{m}_c^{in}$ = 6.92 × 10^{-2} kg s^{-1}; T_c^{in} = 20°C; T_h^{in} = 58°C.

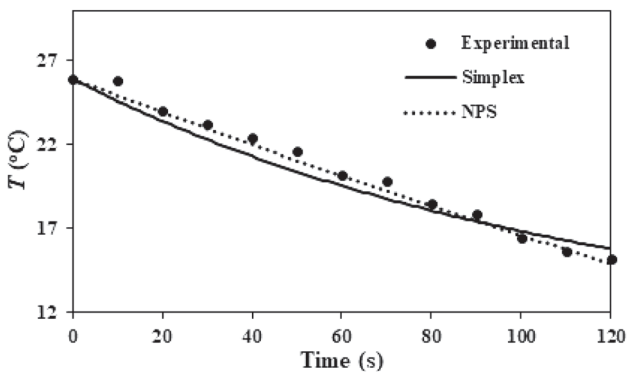

Figure 7. Transient response of cold side outlet temperature of water in the PHE for a negative step change of hot side water flow rate (6.83 − 1.37) × 10^{-2} kg s^{-1} with $\dot{m}_c^{in}$ = 6.94 × 10^{-2} kg s^{-1}; T_c^{in} = 15°C; T_h^{in} = 60°C.

cold water flow rate was 6.93 × 10^{-2} kg s^{-1}. The temperature of the cold side fluid reached close to a steady state at 230 s. The time constant for the response is 94.98 s which is higher than the earlier response. It was observed that the inconsistency to maintain the steady-state at the end of the transient response in figure 4. It was due to the gradual heat gain in the cold-water reservoir. Figure 5 shows the transient response of cold side outlet temperature of water for a positive step change of hot side water flow

rate $(2.74 + 2.74) \times 10^{-2}$ kg s^{-1}, while cold water flow rate was 4.16×10^{-2} kg s^{-1}. The temperature of the cold side fluid came close to a steady state at 230 s. The time constant for the response was estimated as 84.16 s. Figure 6 shows the transient response of cold side outlet temperature of water for a negative step change of hot side water flow rate $(6.84 - 0.27) \times 10^{-2}$ kg s^{-1}, while cold water flow rate was 6.92×10^{-2} kg s^{-1}. The temperature of the cold side fluid reached close to a steady state at 170 s. The time constant for the response was estimated as 95.72 s. The transient response of cold side outlet temperature of water for a negative step change of hot side water flow rate $(6.83 - 1.37) \times 10^{-2}$ kg s^{-1} is shown in figure 7, while cold water flow rate was 6.94×10^{-2} kg s^{-1}. The temperature of the cold side fluid reached close to a steady state at 120 s. The time constant for the response was estimated as 75.10 s.

Table 4 demonstrates the experimental overall heat transfer coefficient of the PHE during transient analysis with its counterparts estimated from the simplex method and NPS method. It is observed that the overall heat transfer coefficient estimated from the simplex methods is lower than that of the NPS method. The simplex method predicted the transient responses with a lower value of the steady states than those of the experimental responses for the positive step changes of flow rate, which are observed in figures 3, 4 and 5. The method predicted a higher value of the steady state for the negative step changes of flow rate in figures 6 and 7. It can be concluded that the simplex method underpredicted the transient response of faster response compared to their experimental counterparts. The time constants for the temperature transients based on the simplex optimization were 50.64 s, 66.44 s, 56.75 s, 90.94 s, and 60.48 s, corresponding to figures 1, 2, 3, 4, and 5, respectively. The simplex optimization results in faster transient responses with lower time constants. The estimated overall heat transfer coefficients with the simplex methods remain lower in the range from 559.83 to 1895.03 W m^{-2} °C^{-1}. It is also observed that the SSE values for the simplex methods are higher than those of the NPS method. The NPS method predicted the experimental transient responses precisely, with quite higher values of overall heat transfer coefficients compared to their counterparts in the simplex method. On the contrary, the NPS method overpredicted the transient response with a slower response compared to their simplex counterparts. The predicted responses with the NPS method belong to the higher values of steady-state in case of the positive step changes of the flow rates which are observed in figures 3, 4 and 5, whereas the method predicted the lower values of steady-state in case of the negative step changes of flow rates in figures 6 and 7. With the slower responses, the estimated overall heat transfer coefficients with the NPS methods remain higher in the range from 1548.45 to 6407.38 W m^{-2} °C^{-1}. In two cases, the NPS methods predicted much higher values of the overall heat transfer coefficients of 2759.55 W m^{-2} °C^{-1} corresponding to figure 7 and 6407.38 W m^{-2} °C^{-1} corresponding to figure 4. It is observed from figures 4 and 7 that the experimental transient responses are not settled to a steady state completely. It was due to some experimental limitations of not providing constant rate heating and cooling during the steady states. The theoretical heat transfer coefficients obtained by the optimized simulation belong to a deviated value of the steady state and it overpredicts the overall heat transfer coefficient. It is mentioned that the experimental heat transfer coefficients belong to the observed steady state values in the figures and the flow rates.

It is interesting to analyze that the NPS predicted a very higher value of the heat transfer coefficient (6407.38 W m^{-2} °C^{-1}) than that of the experimental one with a lower value of SSE 7.7. It is observed that the inconsistency to maintain steady-state at the end of the transient response in figure 4. It was due to the gradual heat gain in the cold-water reservoir of the limited heat capacity. The NPS method converged well to the final state and predicted a higher value of the heat transfer coefficient with the lower SSE. As the NPS method was based on the time-domain ordinary differential equations (Eqs. 23–26), the simulated transients result in the first-order dynamic response. The experimental transients in figures 3, 5, and 6 resemble the first-order response that causes better convergence and lower value of SSE. The estimated heat transfer coefficient obtained by the NPS method for figures 3, 5, and 6 are 1548.45, 2136.86, and 1833.82 W m^{-2} °C^{-1}, respectively with the lower errors. The heat transfer coefficient for figure 5 deviated much from the experimental one because of the inconsistency in the final steady-state during the experimental transient. On the other hand, the experimental transients in figures 4 and 7 resemble close to the second-order response with the time delay. As a result, the NPS method results in higher SSEs and heat transfer coefficients with higher errors. The higher value of the heat transfer coefficients can be attributed to the inconsistency of the experimental responses for figures 4 and 7 in reaching the steady state.

The experimental heat transfer coefficient is more dependent on the flow rate than the temperature. The experimental heat transfer coefficient does not divert much with the temperature deviation of 5°C in the outlet temperature. The experimental heat transfer coefficient remains consistent in all five cases of the transient experiments. On the other hand, the simplex method predicted the heat transfer coefficient with a lower deviation of 6.7% from the experimental one and a higher SSE of 90.95 for figure 4. The simplex method diverged from the experimental data at the end of the transient response that produced the higher value of SSE. However, the divergence favors the actual transient response which the experimental transient lacks. The simplex method with time-domain partial differential equations identifies the inaccuracy and inconsistency of the experiment.

The Nelder-Mead simplex optimization method is a derivative-free nonlinear optimization method based on the estimation of the objective function. It converges well for the uncertain and non-smooth objective functions. For the uncertainty and fluctuating experimental data with changing patterns or trends, complete optimization is impossible rather it requires the overall improvement in the function values. The optimization method quickly improves the minimization process of the objective function within a few iterations. The Nelder-Mead simplex optimization method with time-domain partial differential equations can be accurate if the experimental transient data is smooth with a regular trend. If the transient experimental data contains the discontinuity of trend where an order of the nonlinear pattern changes frequently, the optimization method predicts the unsatisfactory parameters. Figures 6 and 7 contain the fluctuating transient data where the nonlinear pattern changes frequently. In table 4, the predicted heat transfer coefficients with the simplex optimization method corresponding to figures 6 and 7 are 559.83 W m^{-2} °C^{-1} and 438.80 W m^{-2} °C^{-1}, respectively. The simplex optimization method in the two cases predicts the much lower values of heat transfer coefficients than their experimental counterparts.

The simplex method was estimated with the help of the time and space domain partial differential equations (Eqs. 8–11), which results in the second-order dynamics. Here, the space domain was not finely grided control volume with nine nodes along the length of the heat exchanger. If the space domain would be distributed finely with the higher number of nodes, the simplex optimization method would have been converged well to the second-order dynamics.

The simulated transient analysis model was applied for a countercurrent shell and tube heat exchanger facility, and time constants for the cold side responses were evaluated in the range from 120 to 202 s. The temperature response of the shell and tube heat exchanger was slower of higher values of the time constant.

The significant deviations in the transient response were due to both the experimental uncertainty and the measurement uncertainty. The experimental uncertainties were due to the heat losses from the hot reservoir and the heat gain by the cold reservoir during the experimental run. The maximum deviation of temperatures during the repetition of the experiments was ± 2.0°C, whereas the SSE value for the repeatability study was 0.99. The measurement uncertainty was due to the accuracy of the instruments. The uncertainty causes unwanted fluctuations in temperature measurements. The transients obtained by the simplex method deviated from the experimental transients due to the deviations and inconsistency in the experimental data.

There could be good agreement between an optimized heat transfer coefficient and its experimental value if the following constraints would have been overcome with ease during experiments: (1) The cold water and hot water reservoirs should be large enough with a higher heat capacity to produce the minimum temperature fluctuations in the reservoir temperature. It is observed in figure 1 that the outlet streams of cold water and hot water are recycled back to the cold reservoir and hot reservoir, respectively. (2) The reservoir should be insulated and covered to minimize the heat loss that in turn minimizes the temperature fluctuation. (3) The experimental uncertainty should be taken care of.

6. Conclusions

This work extracts the performance parameters based on transient analysis in a plate heat exchanger with the help of experimental technique and the optimized simulations, simultaneously. The overall heat transfer coefficients calculated from the transient experiments are appropriate throughout the flow rate. The transient experiments were limited to the low flow rates of water in the hot and cold sides. The overall heat transfer coefficients were estimated from the parameter estimation techniques based on both the simplex optimization and nonlinear programming solver. The nonlinear programming solver extracted the heat transfer coefficient with lower values of SSE. The simplex method resulted in lower values of heat transfer coefficient than those from the experimental method. The simplex parameter estimation method could be accurate with better convergence if the experimental constraints during a transient experiment would have been overcome with ease.

The time constant of the plate heat exchanger during the transient analysis was lower than that of a shell and tube heat exchanger for the same operating conditions. It will be interesting to analyze the pressure loss coefficients and heat transfer coefficients from transient analysis with a few modifications of the facility and a higher flow rate.

List of symbols

A	Heat exchanger area (m^2)
a	Size of polygon (dimensionless)
b	Mean channel spacing (mm)
C_h	Constant (dimensionless)
c_p	Specific heat (J kg^{-1} °C^{-1})
D_h	Hydraulic diameter (mm)
D_p	Port diameter (mm)
G	Mass velocity (Kg m^{-2} s^{-1})
h	Film heat transfer coefficient (W m^{-2} °C^{-1})
k	Thermal conductivity (W m^{-1} °C^{-1})
L	Length (mm)
m	Mass of fluid in each channel (kg)
$\dot{m}$	Mass flow rate of fluid (kg s^{-1})

N_p Number of plates
n Constant (dimensionless)
P_c Corrugation pitch (mm)
p Plate pitch (mm)
q Number of parameters
p Optimized parameter
Re Reynolds number (dimensionless)
T Temperature (°C)
t Time (s)
U Overall heat transfer coefficient (W m^{-2} $°C^{-1}$)
u Unit vector
v Velocity of fluid (m s^{-1})
w_i Weightage factor for each channel (dimensionless)
X Parameter vector
x Spatial length (m)
z Plate thickness (mm)

Greek symbols

α Coefficient of reflection (dimensionless)
β Coefficient of contraction (dimensionless)
γ Coefficient of expansion (dimensionless)
Δ Differential operator
ϕ Enlargement factor
μ Viscosity (kg m^{-1} s^{-1})
ρ Density (kg m^{-3})
τ Time constant (s)

Subscripts

c Cold side, centroid
cp Channel pass
e Effective, expansion
h Hot side
hor Horizontal
i Number of passes
max Maximum
r Reflection
s Contraction
ver Vertical
w Wall
wd Width

Superscripts

exp Experimental
in Inlet
out Outlet
s Steady state
sim Simulation

Abbreviations

NPS Nonlinear programming solver
PHE Plate heat exchanger
SSE Square sum error

References

[1] Hesselgreaves J E 2001 *Compact Heat Exchangers, Selection, Design and Operation*, Pergamon, Oxford, UK
[2] Kakac S and Liu H 2002 *Heat Exchangers: Selection, Rating and Thermal Design*, 2nd Ed., CRC Press, Boca Raton, FL
[3] Wadekar, V V 2001 Compact exchangers for phase change. HTFS, AEA Technology Hyprotech, Harwell, Oxfordshire
[4] Wadekar V V 2005 Heat Exchangers in Process Industry and Mini-and Microscale Heat Transfer. In: *Proceeding of Fifth Int. conference on Enhanced, Compact and Ultara-Compact Hear Exchangers: Science, Engineering and Technology*, NJ, USA
[5] Cima R M and London A L 1958 The transient response of a two-fluid counterflow heat exchanger-the gas turbine regenerator. *Trans. ASME* 80: 1169–1179
[6] Romie F E 1984 Transient response of the counter flow heat exchanger. *ASME J. Heat Transf.* 106: 620–626
[7] Abdelghani-Idrissi M A, Bagui F and Estel L 2001 Analytical and experimental response time to flow rate step along a counter current flow double pipe heat exchanger. *Int. J. Heat Mass Transf.* 44: 3721–3730
[8] Yin J and Jensen M K 2003 Analytic model for transient heat exchanger response. *Int. J. Heat Mass Transf.* 46: 3255–3264
[9] Mishra M, Das P K and Sarangi S 2006 Transient behaviour of crossflow heat exchangers due to perturbations in temperature and flow. *Int. J. Heat Mass Transf.* 49: 1083–1089
[10] Das S K and Roetzel W 1995 Dynamic analysis of plate heat exchangers with dispersion in both fluids. *Int. J. Heat Mass Transf.* 38: 1127–1140
[11] Das S K, Spang B and Roetzel W 1995 Dynamic behaviour of plate heat exchangers-experiments and modeling. *ASME J. Heat Transf.* 117: 859–864
[12] Rao B P and Das S K 2004 Effect of the flow distribution to the channel on the thermal performance of the multipass plate heat exchangers. *Heat Transf. Eng.* 25: 48–59
[13] Das S K and Murugesan K 2000 Transient response of multipass plate heat exchangers with axial thermal dispersion in both the fluid. *Int. J. Heat Mass Transf.* 43: 4327–4345
[14] Roetzel W and Xuan Y 1992 Analysis of transient behaviour of multipass shell and tube heat exchangers with the dispersion model. *Int J. Heat Mass Transf.* 35: 2953–2962
[15] Srihari N, Rao B P, Sunden B and Das S K 2005 Transient response of plate heat exchangers considering effect of flow maldistribution. *Int. J. Heat Mass Transf.* 48: 3231–3243
[16] Biegler L T, Damiano J J and Blau G E 1986 Nonlinear parameter estimation: A case study comparison. *AIChE J.* 32: 29–45
[17] van der Linde S C, Nijhuis T A, Dekker F H M, Kapteijn F and Moulijn J A 1997 Mathematical treatment of transient kinetic data: Combination of parameter estimation with solving the related partial differential equations. *Appl. Catal. A: General* 151: 27–57
[18] Osman A M and Beck J V 1990 Investigation of transient heat transfer coefficients in quenching experiments. *ASME. J. Heat Transf.* 112: 843–848

[19] Duru O O and Roland N H 2010 Modeling reservoir temperature transients and reservoir-parameter estimation constrained to the model. *SPE Res. Eval. Eng.* 13: 873–883

[20] Khan A I, Billah M M, Ying C, Liu J and Dutta P 2021 Bayesian method for parameter estimation in transient heat transfer problem. *Int. J. Heat Mass Transf.* 166: 120746

[21] Kumar H 1984 The plate heat exchanger: construction and design. In: *The Institution of Chemical Engineers Symposium Series*, 1275–1288

[22] Nelder J A and Mead R 1965 A simplex method for function minimization. *Comput. J.* 7: 308–313

[23] Rao S S 2009 Engineering Optimization Theory and Practice. 4th edn. John Wiley & Sons, New Jersey